

A solid hydraulically amplified piezoelectric microvalve

This article has been downloaded from IOPscience. Please scroll down to see the full text article.

2011 J. Micromech. Microeng. 21 095003

(<http://iopscience.iop.org/0960-1317/21/9/095003>)

View [the table of contents for this issue](#), or go to the [journal homepage](#) for more

Download details:

IP Address: 130.207.50.192

The article was downloaded on 25/08/2011 at 14:09

Please note that [terms and conditions apply](#).

A solid hydraulically amplified piezoelectric microvalve

Xiaosong Wu¹, Seong-Hyok Kim², Chang-Hyeon Ji³ and Mark G Allen⁴

¹ The Dow Chemical Company, Freeport, TX, USA

² LG Electronics, Seoul, Korea

³ Ewha Womans University, Seoul, Korea

⁴ Georgia Institute of Technology, Atlanta, GA, USA

E-mail: XS Wu@dow.com

Received 11 April 2011, in final form 9 June 2011

Published 27 July 2011

Online at stacks.iop.org/JMM/21/095003

Abstract

We report a piezoelectrically driven and hydraulically amplified axial polymer microvalve. The microvalve is normally open and is assembled primarily with stereolithographically fabricated polymer components. An incompressible elastomer is used as a solid hydraulic medium to convert the small axial displacement of a piezoelectric actuator into a large valve head stroke while maintaining a large blocking force. Also, the axial design of the microvalve enables densely packed valve arrays. One application of this microvalve is in pneumatic tactile displays, which operates against gas pressure up to approximately 90 kPa and switching speed between 1 and 200 Hz. The current valve design has a maximum static hydraulic amplification ratio of 5 at 30 V driving voltage and a maximum valve head stroke of 37 μm at 150 V. Under a 94.4 kPa differential pressure, the flow rate of the valve and the closing voltage measure are 785 mL min^{-1} and 150 V, respectively. The function of the microvalve as an on-off switch for a pneumatic microbubble tactile actuator is demonstrated.

(Some figures in this article are in colour only in the electronic version)

1. Introduction

Micromachined valves are crucial components for a wide variety of microfluidic applications. Compared to conventional valves, microvalves have the advantages of finer control of flow rate, relatively faster response, lower production cost, smaller size and lower power consumption. Over the last several decades, significant work has been done on the development of various types of MEMS microvalves. Because of the limitations of micromachining processes and relatively small actuation force and stroke of the valve head, microvalves had limited use in applications that require regulation of flows with high flow rate at high differential pressure. Until recently, the majority of the research effort had been focused on developing microvalves for microfluidic systems that operate under low pressure and require low flow capability at low operating frequency [1–3]. As an example of a microsystem requiring multiple microvalves, pneumatic tactile display application has been demonstrated [4]. In this application, a microbubble actuator is inflated or deflated by

a valved pressurized source. The valves should possess the following characteristics:

- (1) lateral dimension as small as possible so that they can be densely packed to form a full page display;
- (2) ability to work under a large differential pressure of 90 kPa;
- (3) switching frequency up to 200 Hz;
- (4) allowing large flow rate of hundreds of sccm;
- (5) low power consumption; and
- (6) fabrication and packaging process compatible with the fabrication of the polymer pneumatic actuator.

MEMS active microvalves based on a number of actuation methods have been reported, including thermopneumatic [5, 6], thermo-bimorph [7], shape memory alloy [1, 8], electrostatic [9, 10], electromagnetic [11] and piezoelectric [12–21] methods. The thermal actuation methods, including thermopneumatic, thermal bimetallic and shape memory alloy, can potentially achieve large stroke and reasonable actuation force. However, the thermal actuation scheme often exhibits larger power consumption and long response time

than other actuation schemes. High-frequency actuation in the kHz range is also challenging due to the slow response. Electrostatic devices are limited in their deflection and pressure generation capabilities for large actuation force with low voltage operation, because the electrostatic force generated between two parallel electrodes scales inversely with their spacing. Although electromagnetic actuation requires low voltage and the fabrication is straightforward, the concept is impeded by the overall size of the external solenoid and housing structures.

With their high bandwidth, large force and low power consumption, longitudinal d33 mode piezoelectric actuators are promising candidates for driving microvalves at high pressure and high frequency with low-power consumption. Their drawback when used is small stroke (up to 0.1% strain) even at a large applied voltage, which restricts the orifice gap and in turn limits the maximum achievable flow rate. Increasing the piezoelectric film thickness can lead to higher stroke, but at the expense of higher applied voltage. Prior approaches to overcome this drawback include the adoption of a stack-type piezoelectric actuator, piezoelectric bimorph or plate that operates in the transverse d31 mode and hydraulic amplification mechanisms. A leak-proof microvalve was shown to provide large sealing force at a relatively low voltage by using a stack-type piezoelectric actuator, but the stroke was still insufficient for large flow rate applications [12]. A large valve stroke of 80 μm was reported for a piezoelectric bimorph microvalve, but the operation was limited at very low differential pressure [17]. A pneumatic silicon microvalve with a piezoelectric plate actuator was presented to achieve a high flow rate of 2448 mL min^{-1} at a large differential pressure of 600 kPa. However, its large dimension makes spatially dense arrays of valves difficult to realize [22]. A critical problem with the piezoelectric microvalve is to convert the low stroke of a typical piezo stack into a larger stroke valve head movement while maintaining sufficient force. Conventional mechanical transformation means is difficult to realize in a microsystem. Hydraulic amplification primarily based on incompressible liquids is a straightforward method and has been utilized for a long time, but sealing on the microscale is a big fabrication challenge. For example, a hydraulically amplified piezoelectric transducer or lead–zirconate–titanate (PZT) cylinder-driven microvalve was reported with large stroke (20–30 μm), but the fabrication required a complex fabrication process including 22 photolithography steps. [19].

Solid means of hydraulic transmission can be adopted instead of liquid to eliminate the sealing problem while maintaining the advantages of hydraulics on the small scale. In this paper, a simple polymer-based solid-hydraulic amplification (SHA) scheme is used to maximize the stroke of a stacked piezoelectric actuator for a microvalve. An incompressible elastomer is used as a solid hydraulic medium to convert the small axial displacement of a piezoelectric actuator into a large valve head stroke while maintaining a large blocking force. This SHA scheme not only preserves the simplicity of design and fabrication, but also circumvents the sealing problem without losing much efficiency. The piezoelectric stack actuator is vertically integrated with an

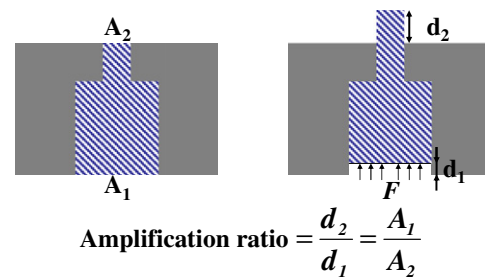


Figure 1. Principle of the SHA mechanism.

amplification chamber, enabling both dense microfluidic functionality and low-voltage operation. Rogge *et al* demonstrated a polymer microvalve with PZT bending disk and SHA, but the PZT disk used had a large lateral dimension that prevented the formation of a dense valve array [20]. In this work, we utilize amplification in the axial direction, making it suitable for forming a dense microvalve array.

2. Concept of SHA

Figure 1 shows the principle of the SHA mechanism. When a force is applied axially to the bottom layer of the hydraulic material, making it undergo a small deflection, the upper surface of the incompressible material undergoes an amplified deflection. The amplification ratio, defined as the ratio of the displacement of the top and the bottom opening, is inversely proportional to the ratio of the areas at top and bottom.

There are two assumptions upon which the SHA concept is based. First, it is assumed that the hydraulic amplification chamber compliance is minimal so that the volume change due to the chamber deformation is negligible. Second, the elastomer is treated as an incompressible material, i.e. the volume change is zero at small deformation.

3. Modeling and design

Consider the case of SHA material in a rigid symmetric chamber as shown in figure 1. Finite element analysis software ANSYS Workbench 11.0, together with analytical models, was employed to study the behavior of the SHA material. As the chamber is symmetric, only one-quarter of each model was simulated in order to minimize simulation time and maximize the number of elements to increase the accuracy. The elastomer material used in the modeling was polydimethylsiloxane (PDMS), which is commonly used in MEMS applications. The constitutive model used was a neo-Hookean model. This model is capable of predicting the stress–strain behavior of materials undergoing large deformations. It consumes less computation time than the more complex Mooney–Rivlin model, yet provides an accuracy equivalent to what the latter does at moderate strain (<33%) [23, 24]. The material properties of structural steel were assigned to the chamber based on the assumption of minimum compliance of the chamber. In addition, all surfaces of the chamber were fixed.



Figure 2. 2D geometry model of a SHA chamber filled with PDMS.

In thermodynamics and fluid mechanics, compressibility is a measure of the relative volume change of a fluid or solid as a response to a pressure (or mean stress) change [25]:

$$\beta = -\frac{1}{V} \frac{\partial V}{\partial P}. \quad (1)$$

The compressibility β is given by the inverse of the bulk modulus K of a material. The bulk modulus K can be defined by the equation

$$K = -V \frac{\partial P}{\partial V}. \quad (2)$$

The inputs for the neo-Hookean model in ANSYS are the initial shear modulus and incompressibility parameter for a hyperelastic material. The shear modulus G can be calculated from

$$G = \frac{E}{2(1 + \nu)}. \quad (3)$$

The relationship between Poisson's ratio ν and incompressibility parameter d is derived below.

The initial bulk modulus

$$K = \frac{E}{3(1 - 2\nu)}. \quad (4)$$

The incompressibility parameter

$$d = 2/K \quad (5)$$

such that

$$d = \frac{6(1 - 2\nu)}{E}. \quad (6)$$

The bulk modulus is a measure of the level of compressibility. The larger the bulk modulus, the higher the required pressure is to make a volume change. As Poisson's ratio approaches 0.5, the bulk modulus of a material approaches infinity, i.e. the material is 100% incompressible, although in reality, no material can be 100% incompressible. To understand the effect of Poisson's ratio on SHA performance, material

Table 1. Shear modulus, bulk modulus and incompressibility parameter from different Poisson's ratios.

	0.49	0.499	0.4999
G (Pa)	6.7114×10^5	6.6711×10^5	6.6671×10^5
K (Pa)	3.3333×10^7	3.3333×10^8	3.3333×10^9
D (1 Pa^{-1})	6.0000×10^{-8}	6.0000×10^{-9}	6.0000×10^{-10}

property constants for PDMS at progressively higher degrees of incompressibility were calculated. Table 1 lists the shear modulus, the bulk modulus and the incompressibility parameter for a PDMS elastomer with a Young's modulus of 2 MPa with various Poisson's ratios. As shown in table 1, the incompressibility decreases by one order with each decimal 9 added to Poisson's ratio. With a Poisson's ratio of 0.4999, the bulk modulus reaches 3.3×10^9 Pa, which is comparable to a 2.2×10^9 Pa bulk modulus of water [26].

In ANSYS simulations, it was found that computing time dramatically increases as Poisson's ratio approaches the value of 0.5. Using a Poisson's ratio of or larger than 0.4999 was not practical for 3D modeling with a fine mesh size. Therefore, a 2D model based on a SHA chamber with a straight slanted side wall, as shown in figure 2, has been constructed in order to use a Poisson's ratio of 0.4999 to ensure the incompressibility in the simulation. In this 2D modeling, all boundary and loading conditions were idealized.

Two different friction boundary conditions between the elastomer and the chamber were applied: bonded and frictionless. With a $1 \mu\text{m}$ displacement applied to the bottom of PDMS, the corresponding top surface displacements were obtained. The ratio of the top displacement to the bottom displacement, or the amplification ratio (AR), was calculated for each friction condition. The simulation results for the two cases are shown in figures 3 and 4, respectively. The insets in figures 3 and 4 are magnified images of the deformed PDMS

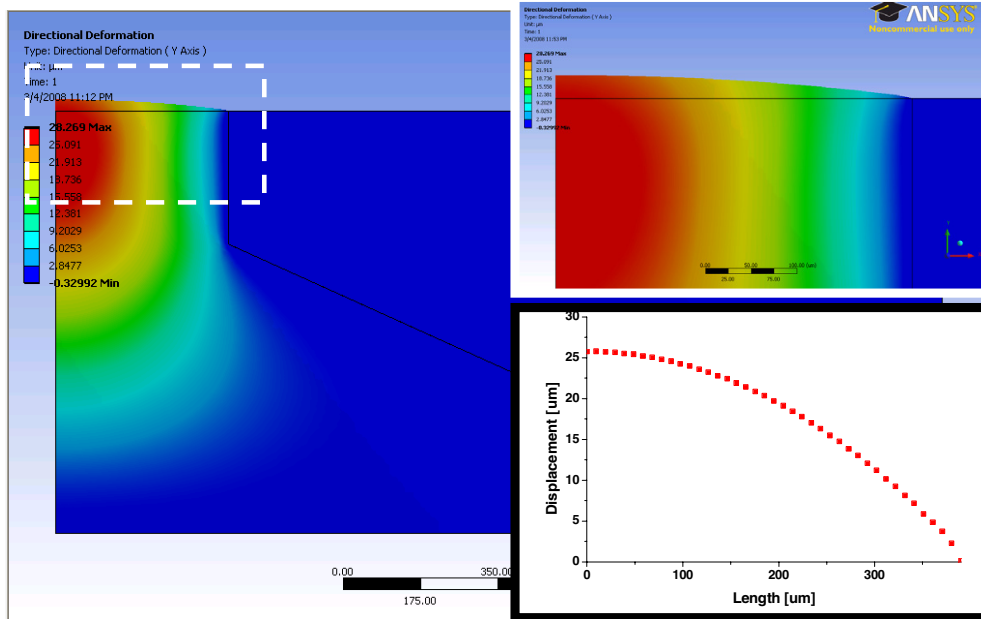


Figure 3. 2D simulation results for the bonded condition between PDMS and the SHA chamber wall.

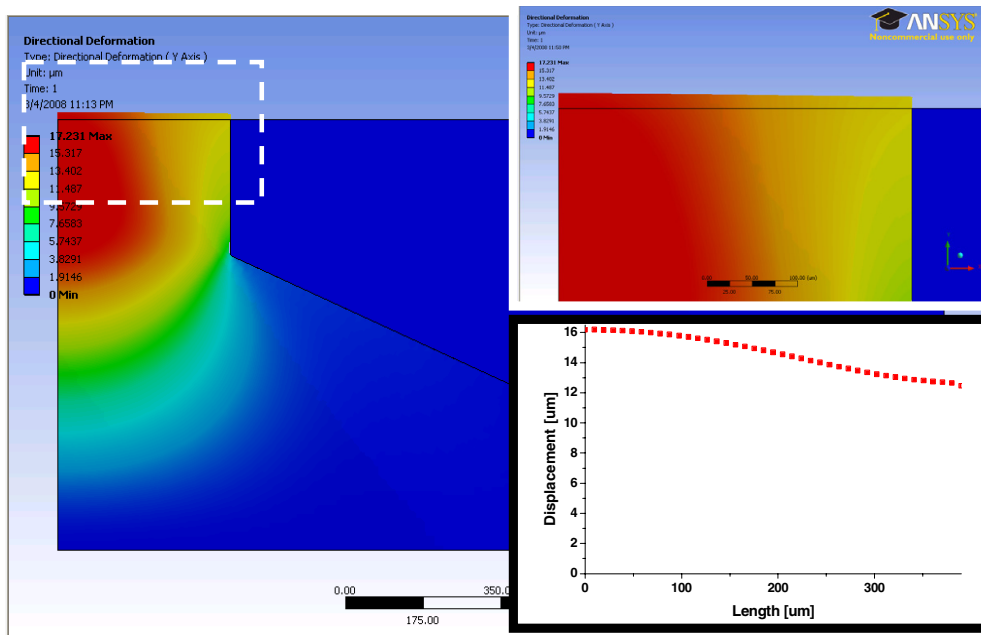


Figure 4. 2D simulation results for the frictionless condition between PDMS and the SHA chamber wall.

at the outlets and the surface profiles of the PDMS. The fully bonded interface results in an arc (spherical) shape and the frictionless interface gives a cylindrical shape with a curved top surface.

The surface profiles of deformed PDMS were used to obtain the volume of the PDMS that had been ‘pushed’ out of the SHA chamber, which was compared with the volume that had been ‘pushed’ into the chamber at the bottom. From this comparison, the volume change of the entire PDMS body can be obtained. Table 2 lists volume analysis results, the displacement results and some important modeling parameters.

The simulation results verified the concept of SHA. The volume of the PDMS is conserved in both cases. Because the deformed PDMS forms a round profile instead of a flat top surface, the top displacement and the amplification ratio are higher than the respective theoretical values.

4. Experimental verification of the SHA concept

One SHA chamber with a calculated amplification ratio of 12.6 was fabricated and assembled with PZT stack actuators. To characterize the assembled actuators, a 0–150 V voltage was applied to the PZT stack actuator, and the deflected shapes of

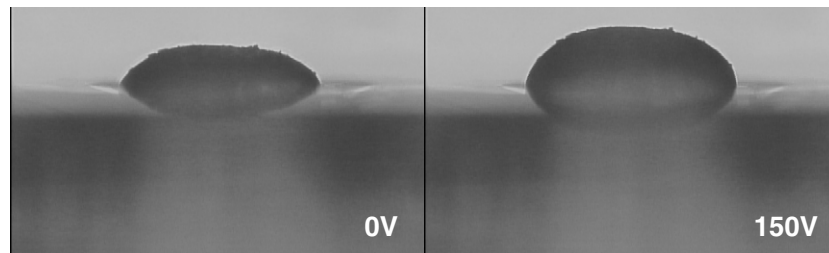


Figure 5. Optical photographs of the deformed PDMS.

Table 2. 2D modeling parameters and results.

Young's modulus of PDMS	2 MPa	
Poisson's ratio of PDMS	0.4999	
Area		
Top	0.478 mm ²	
Bottom	7.069 mm ²	
Theoretical amplification ratio	14.7	
Load displacement	1 μm	
	Bonded	Frictionless
Deformed shape	Spherical	Cylindrical
Displacement		
Max	28.3 μm	17.2 μm
Top	25.8 μm	16.2 μm
Amplification ratio	25.8	16.2
Volume conserved	94.5%	93.9%

the elastomer at the outlet of the SHA chambers were captured using an optical microscope (figure 5). The maximum displacement of the PDMS top surface was measured using a laser sensor. The effects of voltage increase and initial filling of the SHA chamber were studied. As shown in figure 5, the shape of the PDMS deformation agrees well with the fully bonded boundary condition.

Figure 6 shows the theoretical and experimental displacements of the PDMS valve head as functions of the applied voltage. The measured amplification ratio at 50 V is 10, smaller than the theoretical value of 12.6, which would be smaller than the simulated result. The following three factors may have contributed to the discrepancy between the measured value and the predicted value: (1) the modeling and calculation are based on the maximum displacement by the PZT actuator with no load. In reality, there may be a reduction in the PZT displacement due to the stiffness of the PDMS material, which prevents the PZT displacement from reaching its maximum. Especially in this case, the PDMS is pre-deformed and tends to have higher stiffness. (2) As shown in the inset in figure 7, there is PDMS deformation at the gap between the PZT actuator and the bottom edge of the chamber. This 'squeezing out' effect at the bottom of the SHA chamber partially contributes to the loss of volume and thus the decrease in the amplification ratio. (3) The modeling and calculation are based on an ideal case, which does not take into account imperfections such as air bubbles formed in PDMS and the compliance in the hydraulic chamber, two factors that may also result in smaller displacement of the PDMS valve head.

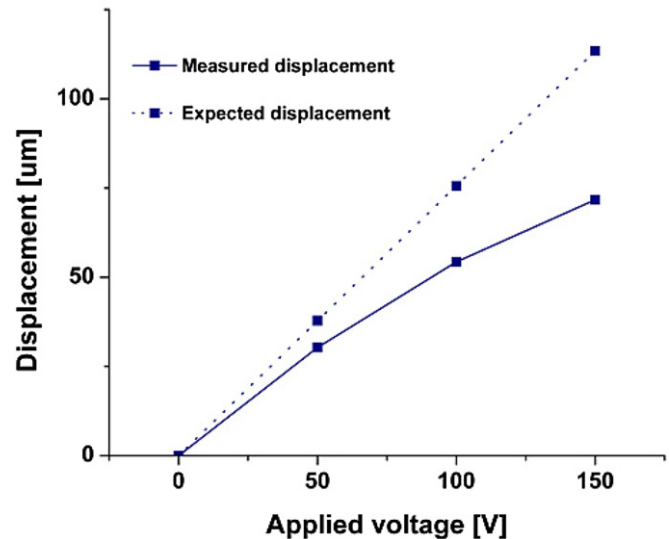


Figure 6. Expected and measured vertical displacement of the actuator as a function of the applied voltage.

Table 3. Actuation characteristics of the actuator compared with theoretical amplification ratio.

Expected amplification ratio	12.6	
Measured characteristics	50 V	150 V
PZT displacement	3 μm	9 μm
PDMS top displacement	30 μm	72 μm
Measured amplification ratio	10	8

In order to reduce the discrepancy between predicted and experimental results, on one hand, the design and fabrication of the SHA chamber can be improved by, e.g., optimizing the contact between the PDMS and the PZT to eliminate any volume loss of PDMS and using a softer PDMS material than Sylgard 184 as the SHA medium. Also, the filling of PDMS prepolymer into the SHA chamber can be improved by minimizing air bubbles and other imperfections. On the other hand, the accuracy of modeling can be enhanced by coupling PZT actuator piezoelectricity with PDMS hyperelasticity, thus taking into account the actual displacement the PZT generates. This coupling may be handled better by the Mooney Rivlin model than the neo-Hookean model.

Table 3 summarizes the measured amplification ratio of the actuator. The actuator achieved amplification ratios of 10 and 8 at applied voltages of 50 and 150 V, which correspond to large vertical displacements of 30 and 72 μm, respectively. The measured displacement deviated from the theoretical

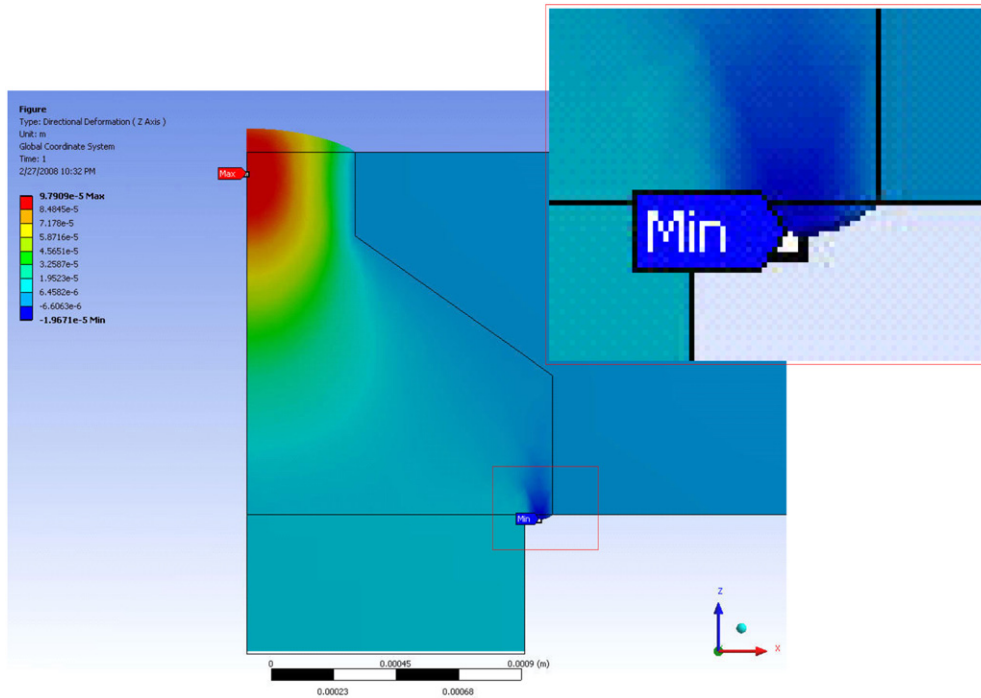


Figure 7. 3D simulation results with the fully bonded condition between PDMS and the SHA chamber wall.

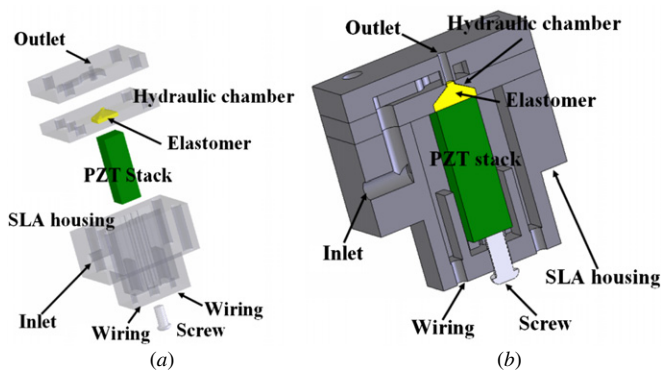


Figure 8. 3D schematics of the microvalve configuration, showing the geometry of the hydraulic chamber and the inlet and outlet paths. (a) Exploded view. (b) Cross-sectional view.

displacement at higher applied voltage in both cases. The higher deviation at higher voltage is attributed to the ‘strain hardening’ effect of PDMS material, the elastic modulus of which increases as strain increases [27, 28].

5. Valve configuration and fabrication

5.1. Valve configuration

Figure 8 shows the exploded and cross-sectional schematics of the designed microvalve with three primary components vertically stacked: a PZT stack actuator as the driving element and the housing; a hydraulic transmission chamber filled with the PDMS elastomer; and a valve chamber connected with an outlet, an inlet and a valve seat.

5.2. Working principle

The operation principle of the microvalve is illustrated in figure 9. The valve inlet has a diameter of 1.5 mm. The valve outlet has a diameter of 0.6 mm with a 100 μm wide valve seat rim. The valve chamber has a rectangular shape and a 1 mm depth. The designed orifice gap is 37 μm between the valve head and the valve seat. Based on the simulation results, the hydraulic chamber has been designed to have slanted sidewalls and vertical offsets at the top and the bottom.

The PDMS serves both as a hydraulic amplification medium and as a valve head. When a voltage is applied to the PZT stack, the PZT stack expands axially and pushes the bottom layer of PDMS upward, generating a small deflection. The PDMS valve head deflects upward at an amplified ratio and stops at the valve seat. Another advantage of using the PDMS elastomer directly as the valve head is its good sealing property [2, 29], especially for the liquid flow. It eliminates the need for a complex valve seat structure normally required for leak-proof valve operation.

5.3. Fabrication

5.3.1. *Stereolithography and layer planarization.* All three primary layers, the valve seat layer, the hydraulic amplification layer and the PZT housing layer, were fabricated primarily using stereolithography (SLA) (Viper Si2, 3D Systems). The contact surface of each layer was finely polished after cleaning and UV post-curing.

5.3.2. *Spacer.* To realize a 37 μm gap of the orifice, a spacer was fabricated by laser cutting a 1.5 mil ($\sim 37 \mu\text{m}$) polyester sheet. The spacer can also be made of a laser micromachined brass sheet in 1.5 mil thickness.

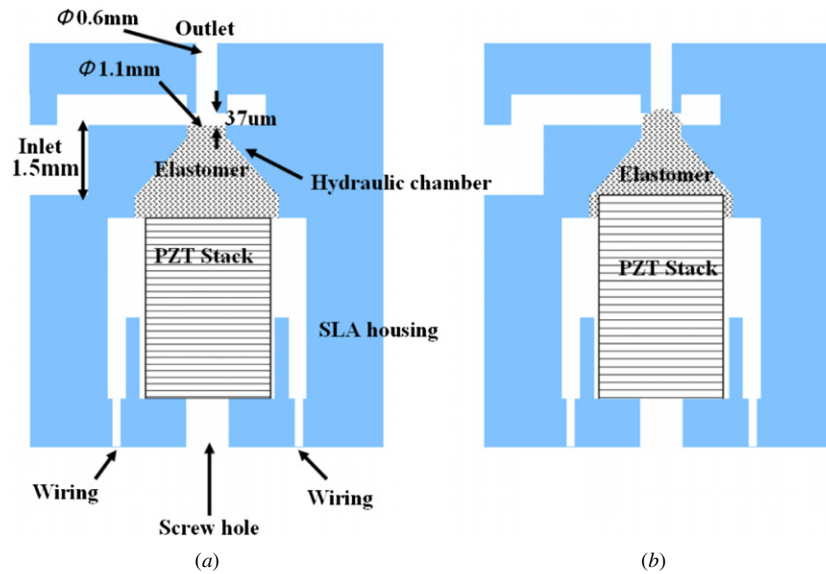


Figure 9. Operating principle of the normally open piezoelectric polymer microvalve. (a) Valve open. (b) Valve closed.

5.3.3. SHA chamber. The hydraulic amplification layer with a hydraulic amplification chamber was bonded to a glass substrate using a wax sheet. A PDMS elastomer base and a curing agent (Sylgard 184, Dow Corning) were mixed well in the 10:1 ratio and degassed. The mixed pre-polymer was then filled into the chamber and vacuum degassed again for 20 min to ensure a complete filling. Curing was conducted at room temperature for 24 h to minimize shrinkage. The hydraulic amplification layer was then released from the glass substrate by dissolving the wax in trichloroethylene (TCE).

5.3.4. Assembly. The PZT stack (Pst $2 \times 3 \times 7$, APC International) with dimensions $2 \text{ mm} \times 3 \text{ mm} \times 9 \text{ mm}$ was assembled in the PZT housing layer. Finally, the housing layer, the hydraulic amplification layer, the spacer layer and the valve seat layer were assembled with four mechanical screws. (Note: for permanent assembly, the screws can be replaced with adhesive bonding, which is compatible with mass fabrication.) The overall dimensions of the fabricated microvalve are $6 \text{ mm} \times 13 \text{ mm} \times 9 \text{ mm}$, as shown in figure 10. The design of the microvalve and the fabrication sequence is compatible with conventional mass-manufacturing technology such as injection molding and lamination at low cost.

6. Characterization

6.1. PZT stack actuator characterization

The static displacement of the assembled PZT stack actuator and the amplified displacement of the PDMS valve head were measured and are plotted in figure 11. Based on these results, the amplification ratio was calculated and are plotted as a function of the driving voltage in figure 12. Three deflection measurements with $0.1 \mu\text{m}$ resolution were performed and the values were averaged for both PZT and amplified PDMS. In this design, the area of the large opening of the hydraulic chamber at the bottom is six times that of the small opening on

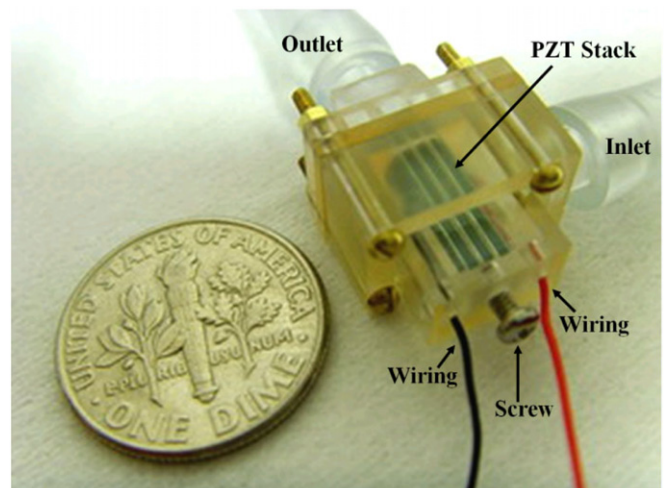


Figure 10. Completely assembled three-layer piezoelectrically driven hydraulically amplified polymer microvalve.

the top. Although the amplification ratio shows a decreasing trend as voltage increases, the amplification ratio is still larger than 4 over the driving voltage range of 0–150 V. A maximum amplification ratio of 5.04 is achieved at 30 V.

The discrepancy between the measured value and the theoretical value of 6, which is calculated based on the device geometry, could have resulted from the factors discussed in previous sections.

6.2. Flow characteristics' measurement

To measure the flow rate, the microvalve was connected to a dc voltage source with 0–150 V of actuation voltage and fed with regulated house N_2 in the range of 0–92.3 kPa. The outlet was connected to a flow meter and maintained at atmospheric pressure. The contact between the PZT stack and the PDMS valve head was realized by adjusting the screw at the bottom of the PZT stack. The gap between the PDMS valve head and

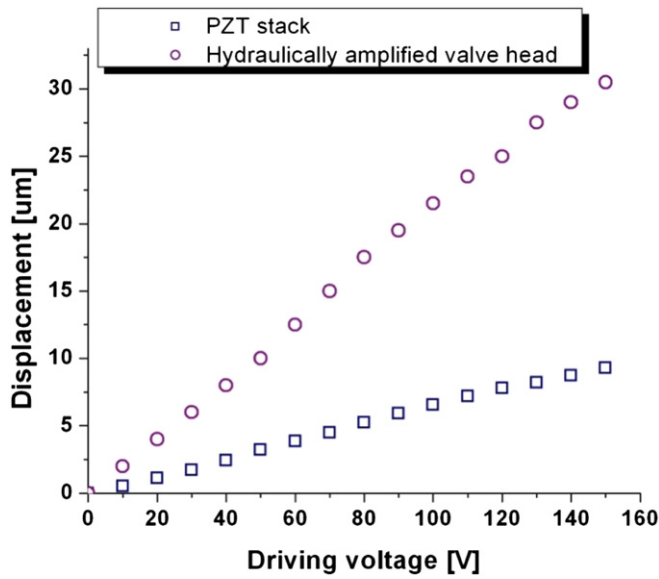


Figure 11. Displacement measurements of the PZT driving element and hydraulically amplified valve head.

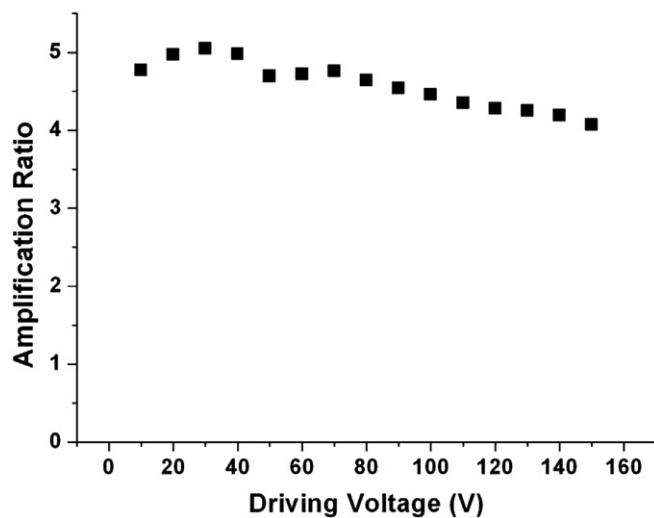


Figure 12. Calculated amplification ratios based on the measured displacement as a function of the driving voltage.

the valve seat was initially adjusted to ensure that the valve would be closed at a maximum allowed driving voltage of 150 V and an inlet pressure of 90 kPa.

Figure 13 shows the flow rate–actuation voltage characteristics of the microvalve under three differential pressures. Because the microvalve is normally open, the maximum flow was obtained without any voltage applied. The maximum flow rates for N₂ at 31.3, 60.5 and 92.3 kPa are 360, 555 and 785 mL min⁻¹, respectively. As the driving voltage increases, the flow rate falls, due to the reduced height of the flow channel and reaches zero when the valve is completely closed. The closing voltages are 130, 140 and 150 V, respectively. Opening voltages are approximately 10 V less than the closing voltages in the cases of 92.3 and 60.5 kPa. At 31.3 kPa, the opening voltage is the same as the closing voltage. Figure 14 plots the flow rates of the microvalve as a

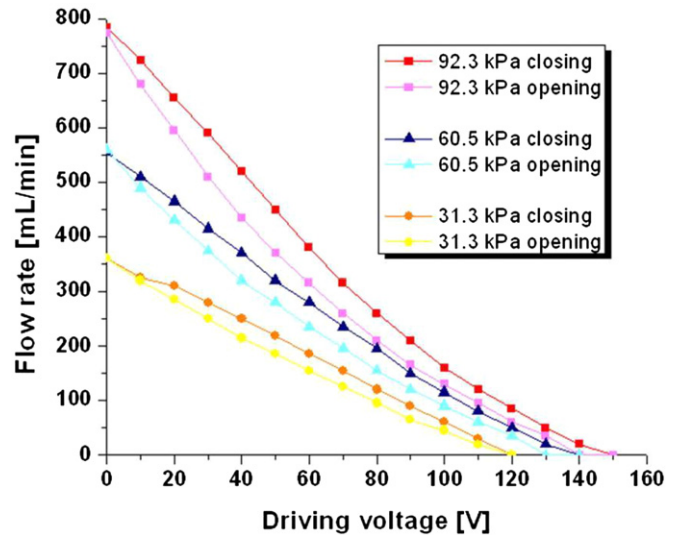


Figure 13. Measured N₂ flow rate as a function of the actuation voltage (dc) under various differential pressures.

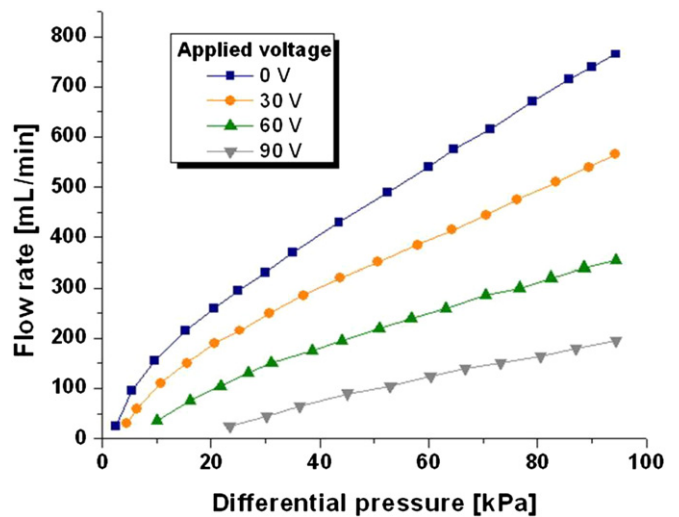


Figure 14. Measured N₂ flow rate as a function of differential pressures at different actuation voltages (dc).

function of the differential pressure at four driving voltages: 0, 30, 60 and 90 V. The curves show some nonlinearity at lower pressure for the cases of 0, 30 and 60 V.

In order to measure the response time of the valve, the outlet was connected to a pressure sensor through a 70 mm long tube with an inner diameter of 3 mm and a throttle, as shown in figure 15(a). The pressure signal is detected at the outlet when the N₂ flow is passing through the valve. The pressure falls to atmospheric when the valve is closed. The control signal and the signal of the pressure sensor were recorded with an oscilloscope. The valve was driven at a frequency of 1 Hz and a voltage of 150 V. The applied pressure at the valve inlet was about 94.4 kPa. Figure 15(b) shows the triggering signal for the microvalve and the signal of the pressure sensor. The delays in sensor triggering for opening and closing the valve appear to be different. The opening valve response time is about 30 ms, and the closing valve response time is about 15 ms. The longer opening response time may have resulted

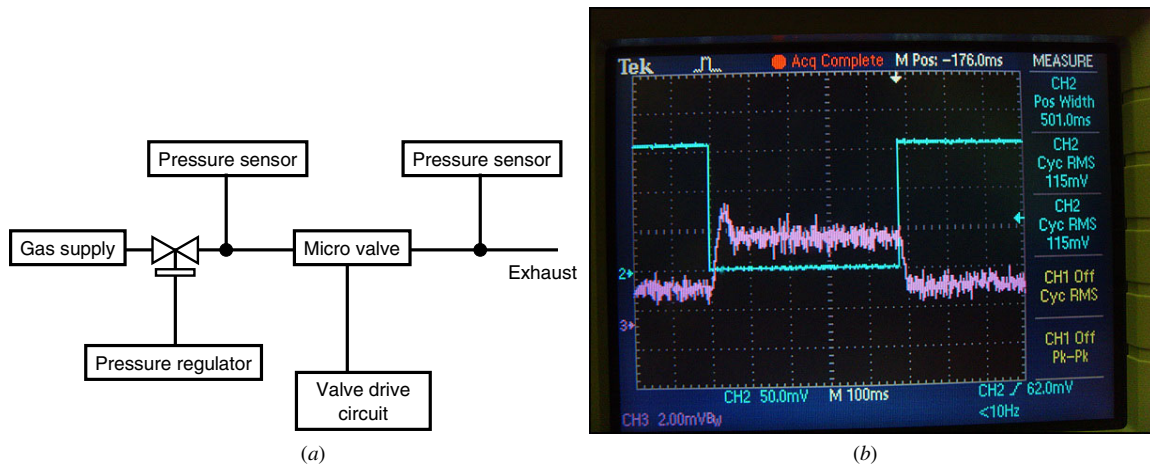


Figure 15. Diagram of valve response time measurement and pictures of the setup, switching time at 94.4 kPa differential pressure and applied voltage of 150 V. (a) Diagram of valve response time measurement. (b) Valve response time.

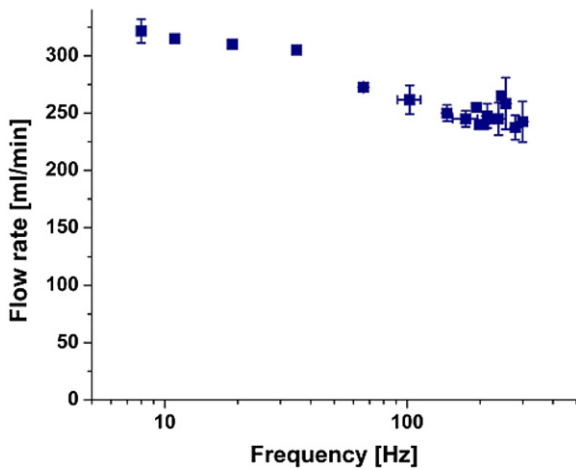


Figure 16. Measured N_2 flow rate as a function of the actuation frequency.

from the sticking of PDMS to the valve seat. PDMS has been known to have stickiness issue due to the tacky low molecular weight oligomers on its surface. The issue is worsened by PDMS’s conformal contact with the valve seat due to its soft and low surface energy nature. A similar sticking phenomenon was observed for a PDMS thermo-pneumatic microvalve which leads to increased delay in response time and hysteresis of the microvalve [2].

Figure 16 presents the measured flow rates of N_2 obtained for valve-operating frequency from 10 to 300 Hz using a sinusoidal actuation voltage with an amplitude of 150 V. The flow rate starts to drop when actuation frequency is higher than 60 Hz. This drop may have been caused by the slow response time of the flow meter at high frequency. Additionally, we tested the hypothesis that the drop is caused by the increases in the elastic modulus and damping factor ($\tan \delta$) of PDMS with increased loading frequency. Specifically, the maximum and minimum displacements of the PDMS valve head as a function of the PZT actuation frequency were measured and plotted in figure 17 together with the relative (i.e. the peak-to-peak difference between maximum and minimum)

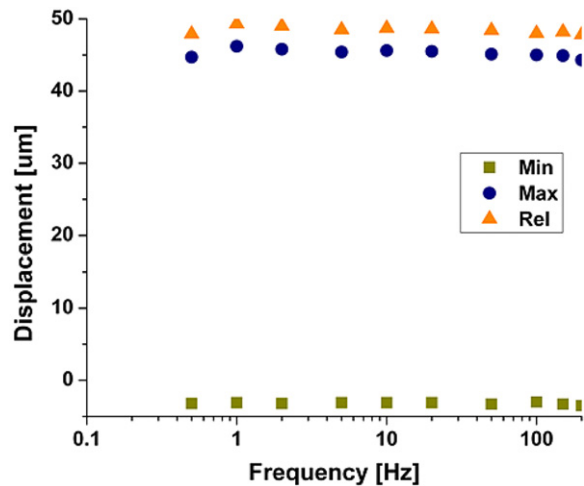


Figure 17. PDMS valve head displacement as a function of the actuation frequency. ‘Min’ refers to minimum displacement; ‘Max’ refers to maximum displacement; and ‘Rel’ refers to relative (i.e. the difference between maximum and minimum) displacement.

displacement. It was found that the displacement of the PDMS valve head remained constant within the frequency range measured, indicating that the microvalve can be fully opened and closed within the frequency range tested. Therefore, we conclude that the flow rate drop at frequency higher than 60 Hz is due to the slow response of the flow meter.

6.3. Demonstration of braille cell driven by a microvalve

The function of the microvalve as an on–off switch for a pneumatic microbubble tactile actuator [4] has been demonstrated in figure 18. The valve was first closed by applying a voltage of 150 V. A differential pressure of 90 kPa was then applied to the inlet of the valve. As shown in figure 18(a), the valve successfully kept the microbubble at the OFF-state. Next, the voltage was turned off and the microvalve was opened. As a result, the microbubble actuator was pressurized (ON-state) and inflated until the pressure reached the level applied to the inlet. Finally, a 150 V voltage

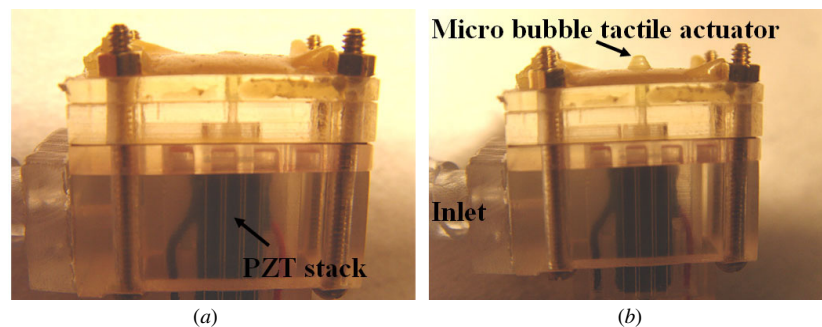


Figure 18. Demonstration of successful control of a tactile actuator for a pneumatic tactile display. (a) Bubble actuator OFF. (b) Bubble actuator ON.

was applied and the valve was closed again. The microbubble actuator remained at the ON-state even after the removal of the inlet pressure (figure 18(b)), which demonstrated the good sealing of the valve.

7. Conclusion

The use of SHA based on the elastomeric incompressible material enables large-stroke, spatially dense arrays of piezo-stack-driven microvalves. The elastomer also acts as the valve head that can be actuated to open and close against a fluid orifice. The behavior and static flow characteristics of the valve subcomponents were evaluated over a range of applied actuation voltage, actuation frequency and differential pressure. The microvalve uses relatively low closing voltages and the adjustable initial orifice gap permits flexible fluid regulation over a large range of differential pressure, i.e. 150 V for 92.3 kPa and 785 mL min⁻¹. Also the proposed axial polymer microvalve can be densely packed and integrated with the miniaturized pneumatic tactile display systems. Although demonstrated in the context of microvalves, the SHA concept shows great promise for other MEMS power transmission applications.

Acknowledgments

The assistance of Richard Shafer of the Georgia Tech Microsensor and Microactuator group on experiments is gratefully acknowledged. This work was supported in part by the National Science Foundation 'Digital Clay' project, contract number IIS-0121663.

References

- [1] Piccini M E and Towe B C 2006 A shape memory alloy microvalve with flow sensing *Sensors Actuators A* **128** 344–9
- [2] Takao H, Miyamura K, Ebi H, Ashiki M, Sawada K and Ishida M 2005 A MEMS microvalve with PDMS diaphragm and two-chamber configuration of thermo-pneumatic actuator for integrated blood test system on silicon *Sensors Actuators A* **119** 468–75
- [3] Vandelli N, Wroblewski D, Velonis M and Bifano T 1998 Development of a MEMS microvalve array for fluid flow control *J. Microelectromech. Syst.* **7** 395–403
- [4] Wu X, Zhu H, Kim S H and Allen M G 2007 A portable pneumatically-actuated refreshable braille cell *Technical Digest of the 14th Int. Conf. on Solid-State Sensors, Actuators and Microsystems, Transducers '07* pp 1409–12
- [5] Henning A K, Fitch J, Hopkins D, Lilly L, Faeth R, Falsken E and Zdeblick M 1997 A thermopneumatically actuated microvalve for liquid expansion and proportional control *Technical Digest of the 9th Int. Conf. on Solid-State Sensors, Actuators and Microsystems, Transducers '97* pp 825–8
- [6] Rich C A and Wise K D 2000 A thermopneumatically-actuated microvalve with improved thermal efficiency and integrated state sensing *Technical Digest of IEEE Solid-State Sensor and Actuator Workshop* pp 234–7
- [7] Jerman H, Sensors I C and Milpitas C A 1990 Electrically-activated, micromachined diaphragm valves *Technical Digest of IEEE Solid-State Sensor and Actuator Workshop* pp 65–9
- [8] Ray C A, Sloan C L, Johnson A D, Busch J D and Petty B R 1992 A silicon-based shape memory alloy microvalve *MRS Proc. Smart Materials Fabrication and Materials for Micro-Electro-Mechanical Systems* pp 161–6
- [9] Shikida M, Sato K, Tanaka S, Kawamura Y and Fujisaki Y 1994 Electrostatically driven gas valve with high conductance *J. Microelectromech. Syst.* **3** 76–80
- [10] Yobas L, Carver B R, Lisy F J and Huff M 1999 A electrostatically actuated MEMS microvalve suitable for pneumatically refreshed Braille-display-system *Proc. Bioeng. Conf.* **42** 85–6
- [11] Capanu M, Boyd J G I and Hesketh P J 2000 Design, fabrication, and testing of a bistable electromagnetically actuated microvalve *J. Microelectromech. Syst.* **9** 181–9
- [12] Chakraborty I, Tang W C, Bame D P and Tang T K 2000 MEMS micro-valve for space applications *Sensors Actuators A* **83** 188–93
- [13] Lee C, Yang E-H, Saeidi S M and Khodadadi J M 2006 Fabrication, characterization, and computational modeling of a piezoelectrically actuated microvalve for liquid flow control *J. Microelectromech. Syst.* **15** 686–96
- [14] Esashi M, Shoji S and Nakano A 1989 Normally closed microvalve and micropump fabricated on a silicon wafer *Sensors Actuators* **20** 163–9
- [15] Yang E-H, Lee C and Mueller J 2003 Normally-closed, leak-tight piezoelectric microvalve under ultra-high upstream pressure for integrated micropropulsion *Proc. IEEE Micro Electro Mechanical Systems* pp 80–3
- [16] Yang E-H, Lee C, Mueller J and George T 2004 Leak-tight piezoelectric microvalve for high-pressure gas micropropulsion *J. Microelectromech. Syst.* **13** 799–807
- [17] Goettsche T, Kohnle J, Willmann M, Ernst H, Spieth S, Tischler R, Messner S, Zengerle R and Sandmaier H 2005 Novel approaches to particle tolerant valves for use in drug delivery systems *Sensors Actuators A* **118** 70–7

- [18] Li H Q, Roberts D C, Steyn J L, Turner K T, Yaglioglu O, Hagood N W, Spearing S M and Schmidt M A 2004 Fabrication of a high frequency piezoelectric microvalve *Sensors Actuators A* **111** 51–6
- [19] Roberts D C, Li H, Steyn L, Yaglioglu O, Spearing S M, Schmidt M A and Hagood N W 2003 A piezoelectric microvalve for compact high-frequency, high-differential pressure hydraulic micropumping systems *J. Microelectromech. Syst.* **12** 81–92
- [20] Rogge T, Rummeler Z and Schomburg W K 2004 Polymer micro valve with a hydraulic piezo-drive fabricated by the AMANDA process *Sensors Actuators A* **110** 206–12
- [21] Weinmann M, Post P, Vollmer H, Wanner R, Kluge S and Woias P 2000 Pneumatic silicon microvalves with piezoelectric actuation *Proc. Actuator* pp 224–7
- [22] Kluge S, Neumayer G, Schaber U, Wackerle M, Maichl M, Post P, Weinmann M and Wanner R 2001 Pneumatic silicon microvalves with piezoelectric actuation *Technical Digest of the 11th Int. Conf. on Solid-State Sensors, Actuators and Microsystems, Transducers '01* pp 924–7
- [23] Treloar L R G 1949 Stresses and birefringence in rubber subjected to general homogeneous strain *Rubber Chem. Technol.* **22** 53–64
- [24] Kofod G 2001 Dielectric elastomer actuators pp 12–5 *PhD Thesis* The Technical University of Denmark
- [25] Beer F P J, Russell E, Dewolf J and Mazurek D 2009 *Mechanics of Materials* (New York: McGraw-Hill) p 56
- [26] Rana A F and Frank J M 1973 Compressibility of water as a function of temperature and pressure *J. Chem. Phys.* **59** 5529–36
- [27] Klimov E, Hoffmann G G, Gumenny A and Siesler H W 2005 Low-temperature FT-NIR spectroscopy of strain-induced orientation and crystallization in a poly(dimethylsiloxane) network *Macromol. Rapid Commun.* **26** 1093–8
- [28] Mark J E 2004 Some interesting things about polysiloxanes *Acc. Chem. Res.* **37** 946–53
- [29] Go J S and Shoji S 2004 A disposable, dead volume-free and leak-free in-plane PDMS microvalve *Sensors Actuators A* **114** 438–44